SAND2016-1374C

Development of glass/steel bibeam specimen for study of brittle crack path stability

S. J. Grutzik[1], E. D. Reedy[2]
[1]Materials Mechanics and Tribology,
Sandia National Laboratories, Albuquerque, NM 87185
[2]Component Science and Mechanics,
Sandia National Laboratories, Albuquerque, NM 87185

1 Abstract

We have developed a novel specimen for studying crack paths in glass. Under certain conditions, the specimen reaches a state where the crack must select between multiple paths satisfying the $K_{\mathrm{II}} = 0$ condition. This path selection is a simple but difficult benchmark case for both analytical and numerical methods of predicting crack propagation. We document the development of the specimen, using an uncracked and instrumented test case to study the effect of adhesive choice and validate the accuracy of both a simple beam theory model and a finite element model. In addition, we present preliminary fracture test results and provide a comparison to the path predicted by two numerical methods (mesh restructuring and XFEM).

Keywords: Brittle fracture, glass, stability, crack path

2 Introduction

Predicting the path along which a brittle crack will propagate is an important but difficult problem. A number of criteria have been proposed since the 1960's to predict crack propagation under mixed mode loading which include maximum hoop stress (or maximum tensile stress) [1], minimum strain energy density [2], and maximum energy release rate [3]. All of these criteria predict that a crack under pure mode I loading will propagate straight ahead. Abstract here In other words, a crack will propagate in a direction such that $K_{\mathrm{II}} = 0$ where K_{II} is the mode II stress intensity factor. The issue of whether a crack path is stable, if a small deviation from the $K_{\mathrm{II}} = 0$ path will bring the crack back in line with the original path or cause further deviation, is a different question. Cotterell and Rice [4] proposed that the $K_{\mathrm{II}} = 0$ path is stable when $T < 0$, where T is uniform tensile stress parallel to the crack direction superposed over the $r^{-1/2}$ asymptotic crack tip field [5]. T is in fact the r^0 term of the asymptotic expansion developed Williams[6]. Yang and Ravi-Chandar [7] have shown the $T < 0$ condition to be of limited applicability. We have developed a novel, thermally loaded specimen which achieves a condition where two independent crack growth directions satisfy the $K_{\mathrm{II}} = 0$ criterion. These paths intersect at a 90° angle and a crack initiated along one can switch to the other with no nominal preference for the crack to turn to the left or to the right. This specimen allows for easy study of the factors controlling crack path stability and the sensitivity of the crack path to various geometrical and material parameters thus providing simple but difficult benchmark case for numerical methods of predicting crack path such as extended finite elements (XFEM)[8] and adaptive remeshing[9].

3 Specimen preparation

The specimens consist of nominally 300 mm beams of borosilicate glass and 304 stainless steel with nominal cross sections 6 mm × 3.17 mm and 6 mm × 31.7 mm respectively joined with an adhesive. Epon 828/Epikure 3140 (100/45 pbw) and U-05FL Hysol urethane adhesive were chosen based on their extremely different mechanical properties and ability to cure at room temperature to test the effect of adhesive choice on specimen behavior. Monofilament nylon spacers were placed in the bond line at the edges of the bars during epoxy curing to provide a uniform bond thickness of approximately 30 µm. After curing, the ends of the bars which included the nylon spacers were cut off to remove any possible stress concentrations in the bond line. To validate the specimen design and ensure negligible impact

of the adhesive on the desired stress state in the bi-material beam an uncracked and instrumented specimen with each adhesive was fabricated. Strain gages were placed on the outer edges of both the bonded glass and steel beams as well as equivalent locations on unbonded reference beams of the same material. Temperature was measured with thermocouples placed near the strain gages on each beam. 350 Ω A type strain gauges were used to best match to the thermal expansion of the stainless steel at temperatures between −30 °C and 30 °C and minimize self heating effects. Specimens were either cooled slowly between these maximum and minimum temperature or in steps of 10 °C held for 1 hour. A schematic of the specimen is shown in Figure 1. For fracture testing, the initial notch was created using a rotary diamond blade. The specimen was held at 45° relative to the blade and cut from both sides to create a chevron notch. During the initial loading this chevron fills first resulting in a sharp crack front. A schematic of the notched specimen is shown in Figure 2.

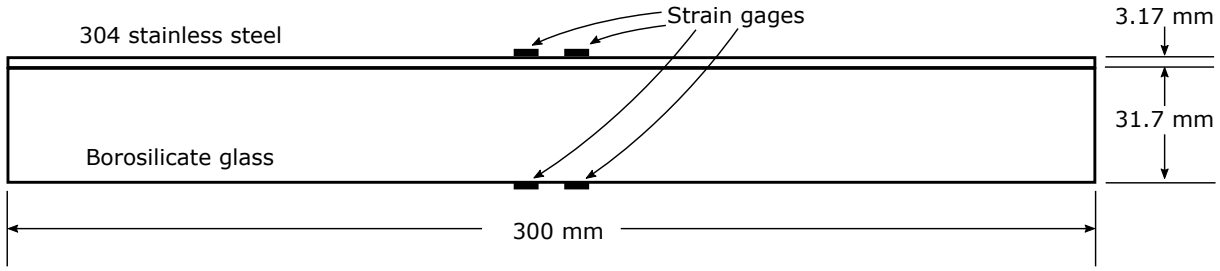

Figure 1: Schematic of the bibeam specimen with strain gage locations indicated

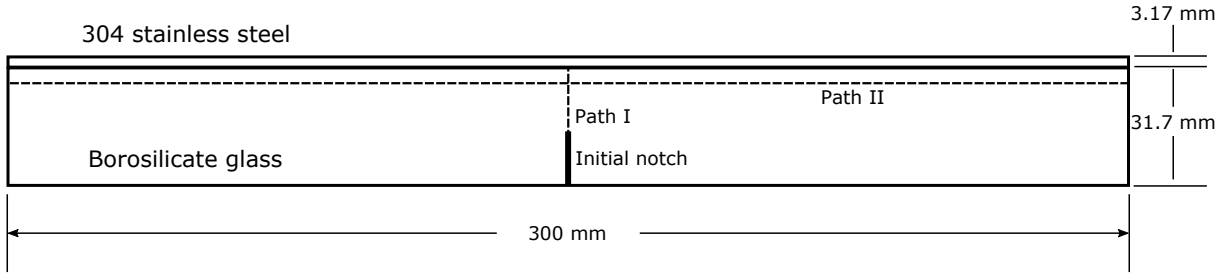

Figure 2: Diagram of the glass/metal bibeam specimen showing the initial notch location and two paths satisfying $K_{\mathrm{II}} = 0$

4 Strain gage calibration

Strain gage output is temperature sensitive due to the temperature dependence on the resistivity of the gage materials and thermal mismatch between the gage and the test sample. Gages are provided with a calibration to account for this sensitivity, however the calibration and gage design is optimized for a particular structural material (usually steel) and a range of test test temperatures near room temperature [10, 11].

A preliminary check on strain gage accuracy through the temperature range used in these tests can be obtained using the strain gage output on the unbonded reference bars alone. If the output of the gage on the glass reference bar is subtracted from that of the gage on the steel reference bar, the result is the difference in thermal expansion. The slope of the resulting curves can be compared to the difference in CTE of the two materials. This comparison is shown in Figure 3. Two gages placed on both the glass and steel, resulting in measured CTE differences of 12.4 µm/m/°C and 12.6 µm/m/°C. The difference between accepted CTE values is 14.1 µm/m/°C. The CTE difference measured by the two sets of gages was 2.4 %. A comparison of the measured and accepted CTE values for glass and steel yielded an average difference of 11 % between those values. The agreement between the accepted and measured differences was regarded as sufficient, effectively qualifying the strain gages for the crack crack growth study

5 Adhesive selection

Preliminary characterization through strain gage instrumentation and photoelastic stress measurements indicated that the adhesive could impact the stress distribution in the bi-material beams. A small study was performed to

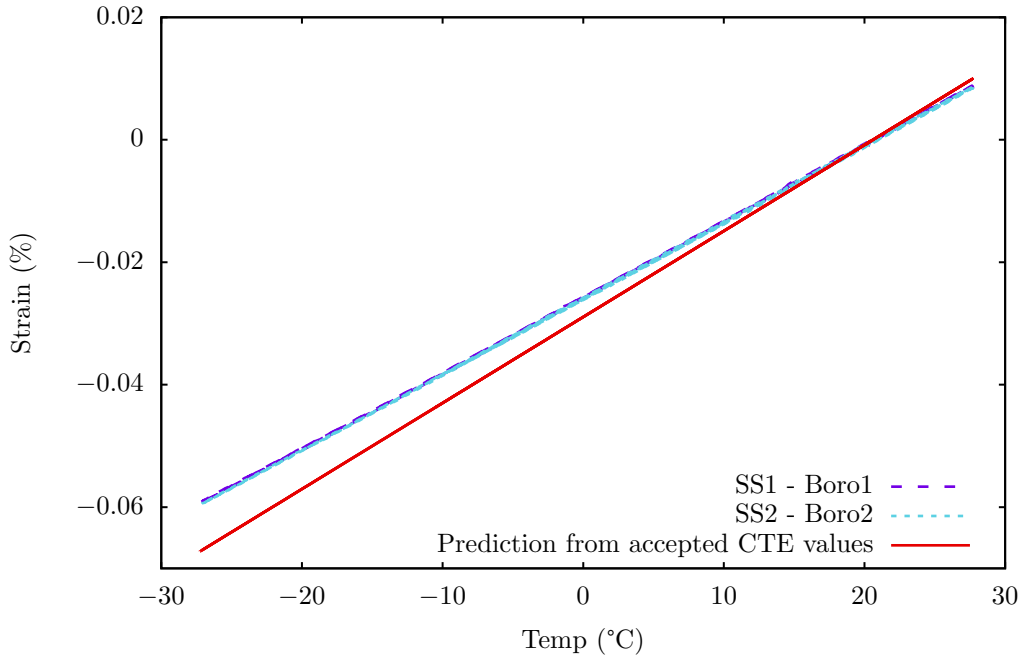

Figure 3: Difference in thermal expansion as measured by strain gages on reference materials as well as the prediction from accepted values

optimize the application of the adhesive such that its impact on the stress distribution of the bi-material beams was minimized. Bibeam specimens were made with two different adhesives; the above mentioned Epon 828/Epikure 3140 epoxy and U-05FL Hysol urethane adhesive. Compared to the Epon/Epikure epoxy, the Hysol urethane adhesive provides a better bond to the glass surface but is significantly more compliant. A bibeam specimen with each adhesive was prepared and instrumented with strain gages and thermocouples as described above and illustrated in Figure 1. The bibeam specimens were simultaneously cooled to −30 °C producing the strain gage results shown in Figure 4, where E Bi is a bibeam with the Epon epoxy and U Bi is a bibeam with the Hysol urethane adhesive. Even though the adhesive layer is thin (about 30 µm as set by the nylon spacers), the response of the bibeam is quite different between the two adhesives. A finite element model was used to further understand the effect of adhesive choice on bibeam performance. Figure 5 shows finite element calculated strains at the glass surface with both adhesives modeled as either a linear elastic or Neo-Hookean [12] hyperelastic material. The linear elastic moduli and CTEs used in the finite element model are listed in Table 1. The Neo-Hookean parameters for the two adhesives are listed in Table 2. The bibeam geometry used in the simulations was slightly different than the bibeam used to produce the experimental result give in Figure 4. Thus, the magnitude of the strain provided by the simulations was not expected to provide a direct match with that experimental result. From Figure 5, we see that the adhesive choice has a large effect on the response of a bibeam. The results show that not only does a compliant adhesive impact the bibeam response but the constitutive details of the compliance have a magnified effect on bibeam response. Furthermore, it is apparent that the details of the constitutive response of the Epon can be neglected when calculating stresses and strains. For these reasons, it was decided that all future bibeams will be made with the Epon epoxy rather than the Hysol urethane adhesive, even though the bond strength is weaker.

Table 1: Material properties for bibeam materials with U-04FL estimated to be 100 times more compliant than Epon 828

	E (GPa)	ν	CTE (µm/m/°C)
Borosilicate Glass [13]	64	0.2	3.25
304 Stainless Steel [14]	193	0.29	17.3
Epon 828/Epikure 3140 epoxy [15]	2.9	0.4	NA
U-04FL Hysol urethane adhesive	0.029	0.45	NA

Table 2: Neo-Hookean parameters for the two adhesives with Epon 828 C_{10} estimated from a tensile strength of 8.5 ksi and elongation at failure of 4.5 % [15] and D_1 as $10 \cdot C_{10}$ and U-04FL estimated as 100 times more compliant than Epon 828

	C_{10} (MPa)	D_1 (MPa)
Epon 828/Epikure 3140 epoxy	166	1660
U-04FL Hysol urethane adhesive	1.66	16.6

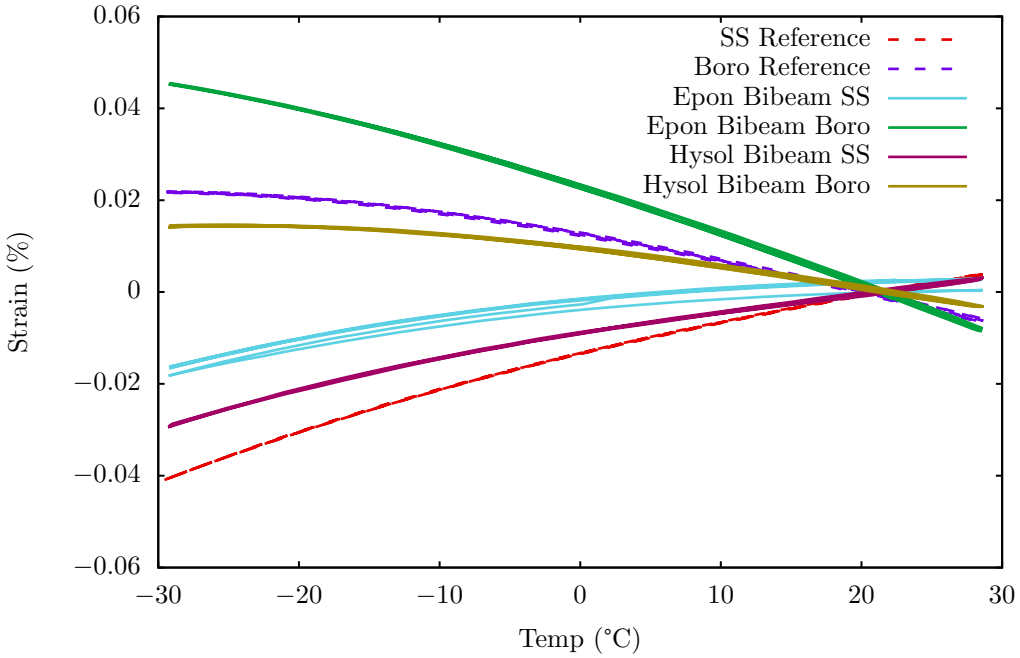

Figure 4: Raw strain gage output for bibeams with Epon epoxy (E Bi) and Hysol urethane adhesive (U Bi) as well as unbonded glass and steel reference bars

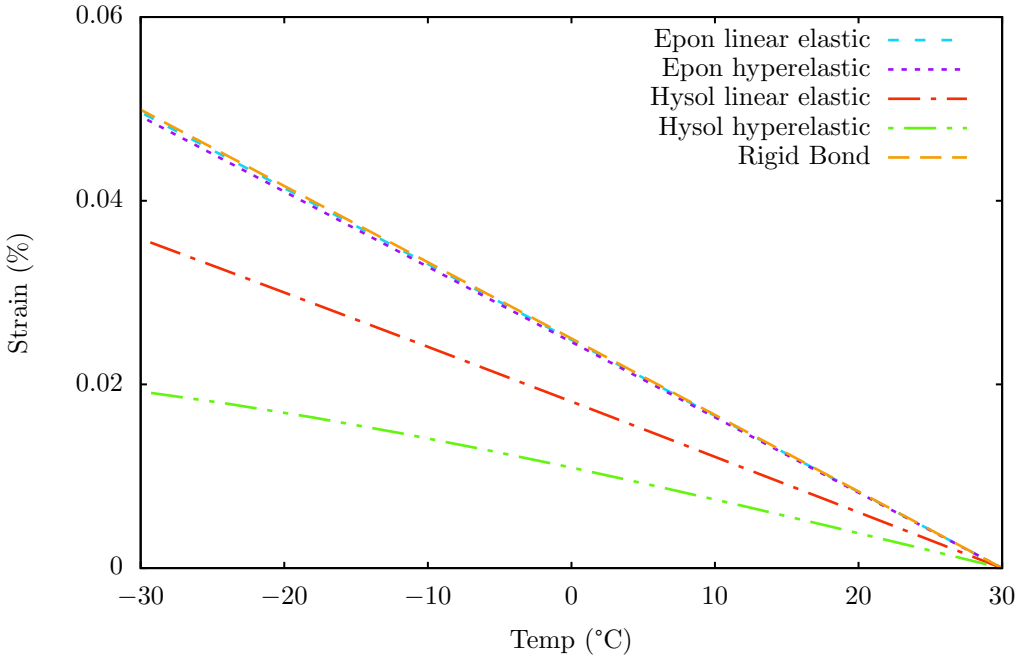

Figure 5: Finite element calculated stress and strain for a bibeam with either Epon epoxy or Hysol urethane adhesive modeled as both linear elastic or Neo-Hookean hyperelastic material as well as assuming a rigid bond at the interface

6 Validation of bibeam with Epon epoxy

If the Epon adhesive layer is assumed to be a rigid bond, the layer can be neglected and a bibeam specimen with no cracks can be modeled using Euler-Bernoulli beam theory. As a final validation, a bibeam specimen was made with the Epon epoxy and two nominally identical strain gages from the same package were placed at each measurement location. If the output of a gage at an equivalent location on an unbonded reference bar is subtracted from the output of a gage on the bibeam, the result is linear in temperature and can be compared with Euler-Bernoulli beam theory prediction. The comparison is shown in Figure 6. The strain as calculated with Euler-Bernoulli beam theory is also shown. There is a 5.1 % difference between the two gages on the steel beam. An error occurred with one of the gages on the glass beam such that no measure of repeatability can be found for gages on the glass. There is an average difference of 14.3 % between the gages on the steel and the beam theory prediction and an error of 5.3 % between the gage on the glass and the beam theory prediction. The larger difference in the beam theory of the gage on the steel can be accounted for by the larger relative uncertainty of the dimensions of the thin steel beam.

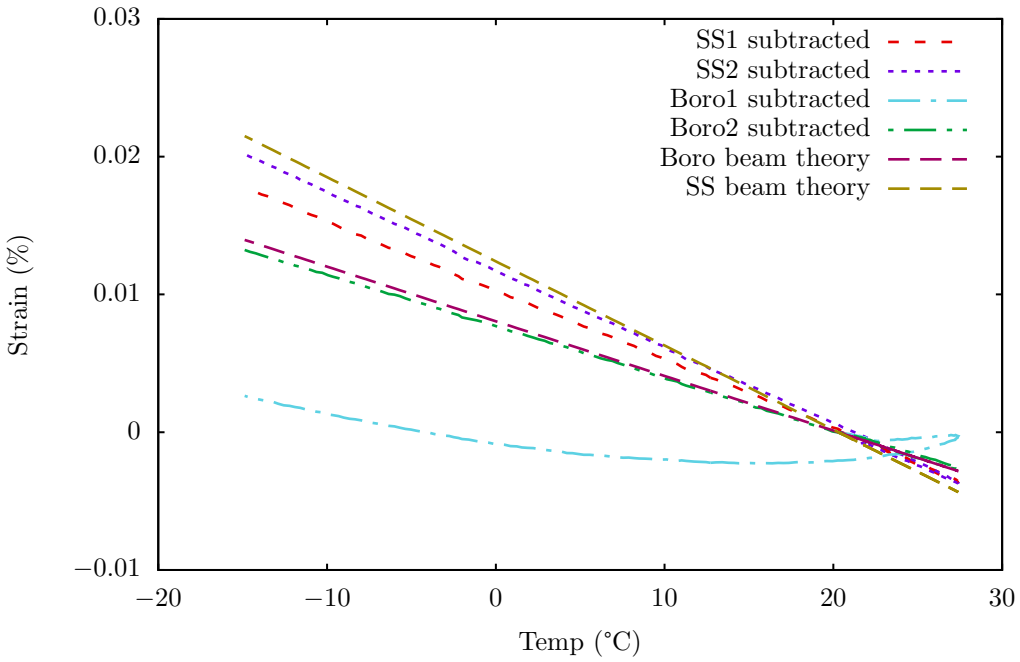

Figure 6: Corrected strain gage output on the glass and steel parts of the bibeam along with beam theory predictions

7 Fracture testing procedure

During testing the specimen is cooled from room temperature. The difference in CTE between the steel and the borosilicate puts the specimen in bending. Figure 7 shows finite element calculated energy release rate as a function of crack length if the crack is started from the bottom in the middle of the specimen, as depicted in Figure 2. Energy release rate is shown both with a straight crack and a small 90° kink at the crack tip with kink length 1 % of the nominal crack length. If the initial crack is more than roughly half width of the glass, energy release rate for the straight crack decreases with increasing crack length and the crack propagates stably with further loading (decreasing temperature).

Due to the placement of the cooling fan there is a slight temperature gradient in the testing chamber. To counteract this, the specimen is suspended freely inside a secondary chamber made of clear acrylic. The secondary chamber removes any convective cooling effect from the fan and results in a uniform temperature distribution along the length of the specimen. Specimen temperature is tracked with a thermocouple placed on the surface of the glass. The stress field around the crack tip is visualized via the photoelastic effect [16]. This gives a precise location of the crack tip and eventually will allow stress intensity factors and T-stress to be extracted directly from the photoelastic image. The arrangement of the photoelastic polariscope is depicted in Figure 8.

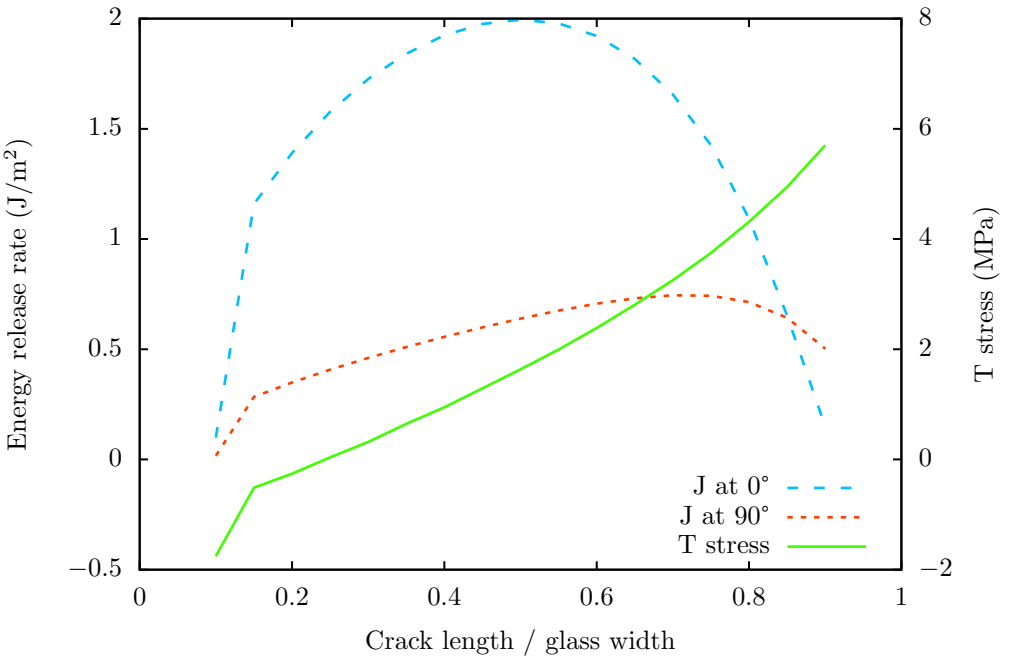

Figure 7: T stress and energy release rate as a function of crack length

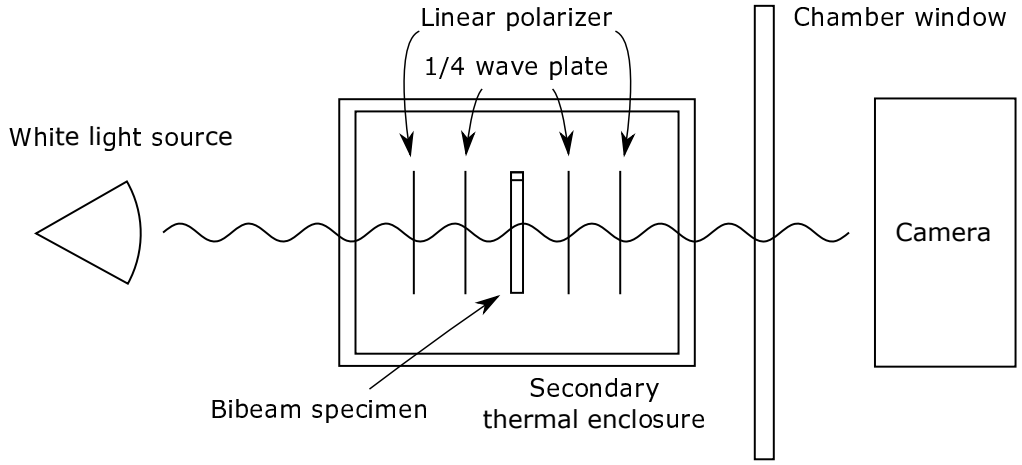

Figure 8: Diagram showing the arrangement of the polariscope used for crack path observation

8 Fracture testing results

A series of photoelastic images as the crack propagates during cooling is shown in Figure 9. A numerical method to track the crack tip in each image frame and extract the stress intensity factors and T-stress [17] is currently in development. As the crack tip approaches the steel, the crack path becomes unstable and the crack growth direction switches to the alternate $K_{\mathrm{II}} = 0$ path parallel to the interface (as depicted in Figure 2). As the crack tip approaches the steel the initial crack path becomes unstable (although it still satisfies $K_{\mathrm{II}} = 0$) and the crack switches to the alternate path parallel to the interface. The distance between this second crack path and the interface matches that predicted for steady state cracking in a brittle substrate by Suo and Hutchinson [18]. If the crack is initiated at the center of the specimen the stress field is nominally symmetric about the crack tip and there is no preference to it turning left or right.

The cause of this behavior is suggested by the energy release rate curves in Figure 7. Along with energy release rate for a straight crack, Figure 7 also shows energy release rate with a small 90° kink at the end of the crack and T-stress. When the crack nears the glass/steel interface, energy release rate of the kinked crack (parallel to the interface) becomes greater than the energy release rate of the straight crack. This suggests the straight crack is no longer stable beyond this point and any small deviation from a straight path will cause it to continue to turn until the crack is propagating parallel to the interface. T-stress is positive during the entire process, except for very small initial notches. The Cotterell and Rice $T > 0$ criterion for crack path instability is thus satisfied at all times and is overly conservative in this case since path instability only occurs near the interface. If the crack is initiated near the end of the specimen, the stress field is not symmetric and the crack always turns toward the interior of the specimen at a larger radius. This is shown in Figure 10.

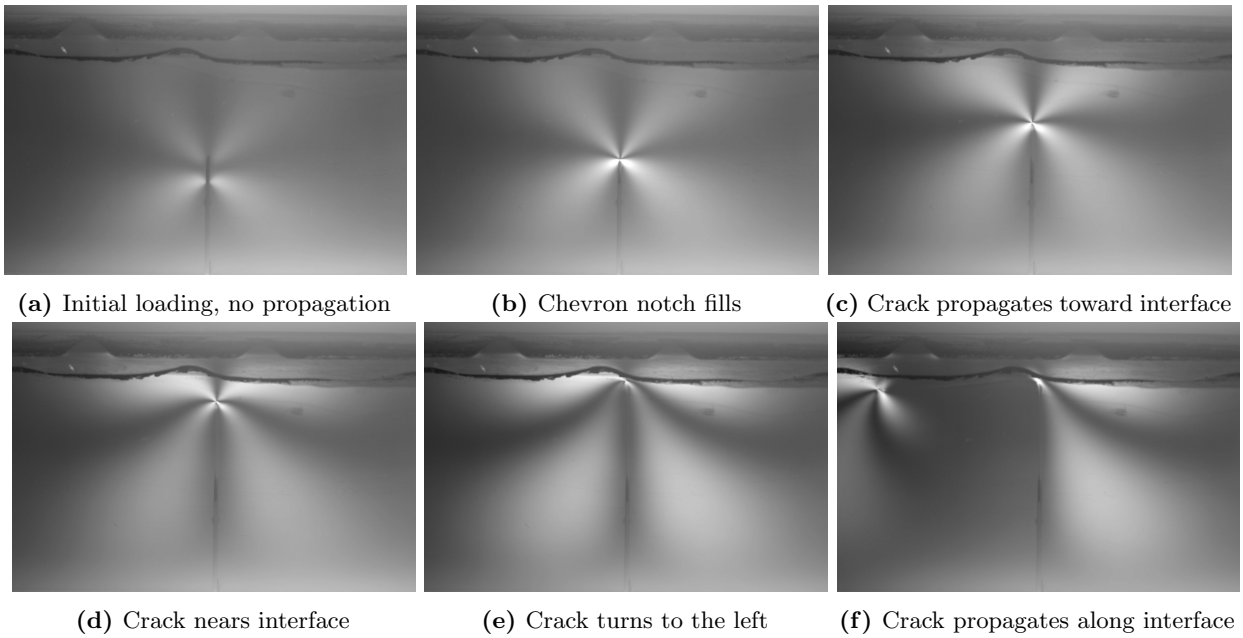

(a) Initial loading, no propagation **(b)** Chevron notch fills **(c)** Crack propagates toward interface

(d) Crack nears interface **(e)** Crack turns to the left **(f)** Crack propagates along interface

Figure 9: An example of a crack propagation sequence with the crack tip highlighted by photoelasticity

9 Comparison with numerical crack propagation calculations

Some initial attempts have been made to numerically predict the crack path in the asymmetric case where the crack is initiated near the end of the specimen. The specimen shown in Figure 10 where the notch is located near the end of the specimen was modeled using the XFEM capabilities of the commercial FEA code ABAQUS[19] and Sandia's SIERRA/SolidMechanics[20] used in conjunction with the commercial fracture code FRANC3D[21]. XFEM models cracks without mesh restructuring, calculating the crack faces within each element with nodal shape functions. FRANC3D[21] uses adaptive mesh restructuring to incrementally advance a crack through a model. The crack path predicted by each method is shown in Figure 11. The SIERRA/FRANC3D result not only qualitatively matches the

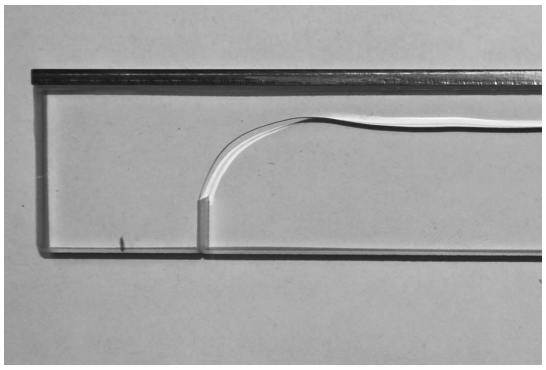

Figure 10: Crack propagating from a notch located near the end of a bibeam specimen

experiment (shown in Figure 10) but the final distance of 4.9 mm between the crack and the glass/metal interface agrees with an analytical model of substrate cracking [18]. In contrast, ABAQUS with XFEM predicts the crack turning parallel to the interface much too early.

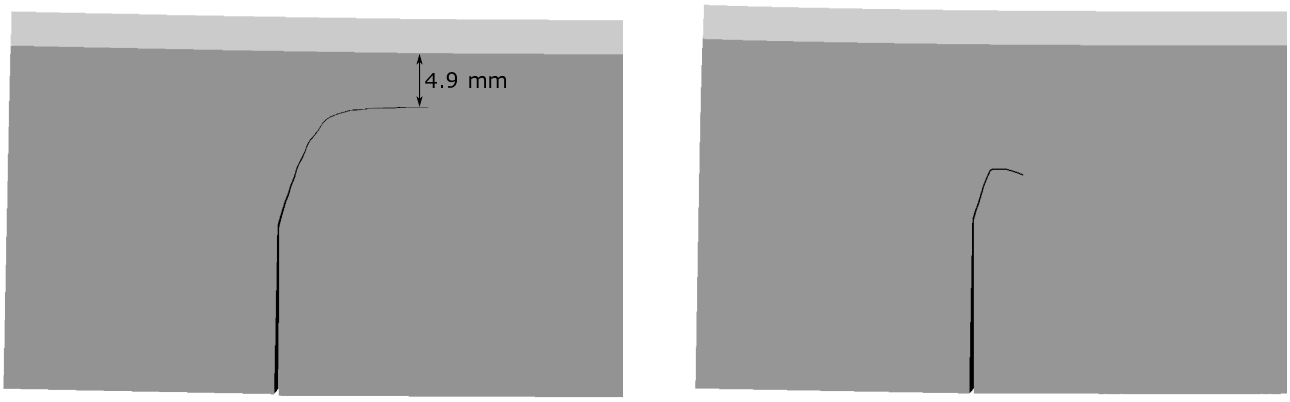

Figure 11: Simulation of crack propagation in an end-notched specimen with SIERRA/SM with FRANC3D (left) and ABAQUS with XFEM (right)

10 Conclusions

Bibeam specimen geometry has been optimized and its behavior validated for fracture-based experiments using strain gage measurements. Although a small differences exists between the strain gage results and beam theory they can be attributed to uncertainty in thermal response and repeatability of the strain gages and spread in reported values for elastic moduli and CTE for the materials involved. While strain gages should be fairly repeatable under the right circumstances, at temperatures outside the ideal range and on materials the strain gage is not compensated for, the thermal behavior is complicated and highly temperature dependant. Data on repeatability of thermal effects in strain gages is sparse to nonexistent. Nonetheless, we feel that the spread of gage output relative to each other and predictions from accepted material parameters and beam theory are reasonable given the factors involved. A experimental method providing stable crack propagation through the borosilicate has also been developed. This method allows for the effect of specimen geometry and material parameters to be investigated and comparisons can be made to numerical crack prediction methods.

Acknowledgements

The authors thank Garth Rohr and Corey Gibson for assistance with experiments and John Laing for valuable strain gage discussions. Sandia National Laboratories is a multi-program laboratory managed and operated by Sandia Corporation, a wholly owned subsidiary of Lockheed Martin Corporation, for the U.S. Department of Energy's National Nuclear Security Administration under contract DE-AC04-04AL85000.

References

[1] F. Erdogan and G. C. Sih, "On the crack extension in plates under plane loading and transverse shear," *J of Basic Engineering*, vol. 85, pp. 516–527, 1963.

[2] G. C. Sih, *Mechanics of Fracture*, vol. 1. Springer, 1972.

[3] C. W. Wu, "Maximum energy release rate criterion applied to a tension-compression specimen with crack," *J Elast*, vol. 8, no. 3, pp. 235–257, 1978.

[4] B. Cotterell and J. R. Rice, "Slightly curved or kinked cracks," *Int J Fract*, vol. 16, no. 2, pp. 155–169, 1980.

[5] M. Gupta, R. C. Alderliesten, and R. Benedictus, "A review of T-stress and its effects in fracture mechanics," *Eng Fract Mech*, vol. 134, pp. 218–241, 2015.

[6] M. L. Williams, "On stress distribution at base of stationary crack," *J Appl Mech*, vol. 24, no. 56, pp. 109–114, 1957.

[7] B. Yang and K. Ravi-Chandar, "Crack path instabilities in a quenched glass plate," *J Mech Phys Solids*, vol. 49, no. 1, pp. 91–130, 2001.

[8] N. Moës, J. Dolbow, and T. Belytschko, "A finite element method for crack growth without remeshing," *Int J Numer Methods Eng*, vol. 46, no. 1, pp. 131–150, 1999.

[9] T. N. Bittencourt, P. A. Wawrzynek, A. R. Ingraffea, and J. L. Sousa, "Quasi-automatic simulation of crack propagation for 2D LEFM problems," *Eng Fract Mech*, vol. 55, no. 2, pp. 321–334, 1996.

[10] Micro-Measurements, "Measurement of thermal expansion coefficient using strain gages," Tech. Rep. TN-513-1, Vishay Precision Group, 2010.

[11] Micro-Measurements, "Strain gage thermal output and gage factor variation with temperature," Tech. Rep. TN-504-1, Vishay Precision Group, 2014.

[12] SIMULIA, *ABAQUS Analyis User's Guide*, 6.14 ed., 2014. Section 22.5.1.

[13] Corning, Inc, "Properties of PYREX®, PRYEXPLUS®, and low actinic PYREX code 7740 glasses."

[14] A. I. H. Committee, *Metals Handbook*, vol. 1. ASM International, 10 ed., 1990.

[15] Hexion, "Technical data sheet, Epikure™curing agent 3140." www.hexion.com/Products/TechnicalDataSheet.aspx?id=2654, August 2007.

[16] K. Ramesh, *Digital Photoelasticitiy*. Springer, 2000.

[17] V. K. Singh and P. C. Gope, "Experimental evaluation of mixed mode stress intensity factor for prediction of crack growth by photoelastic method," *J Fail Anal and Preven*, vol. 13, pp. 217–226, 2013.

[18] Z. Suo and J. W. Hutchinson, "Steady-state cracking in brittle substrates beneath adherent films," *Int J Solids Struct*, vol. 25, no. 11, pp. 1337–1353, 1989.

[19] SIMULIA, *ABAQUS Analyis User's Guide*, 6.14 ed., 2014.

[20] Sandia National Laboratories, *Sierra/SolidMechanics User's Guide*, 4.38 ed., 2015.

[21] Fracture Analysis Consultants, Inc, *FRANC3D Reference Manual*, 7 ed., 2016.